J Intell Robot Syst (2016) 81:301–316
DOI 10.1007/s10846-015-0225-z

Humanoid Posture Selection for Reaching Motion and a Cooperative Balancing Controller

Inho Lee · Jun-Ho Oh

Received: 12 October 2014 / Accepted: 16 February 2015 / Published online: 16 May 2015

Abstract Our goal in this research was to develop a motion planning algorithm for a humanoid to enable it to remove an object that is blocking its path. To remove an object in its path, a humanoid must be able to reach it. Simply stretching its arms, which in a humanoid are shorter than its body and legs, is not sufficient to reach an object located at some distance away or on the ground. Therefore, reachability has to be ensured by a combination of motions that include kneeling and orienting the pelvis. However, many posture selection options exist because of the redundancy of a humanoid. In this research, we focused on the optimization of the posture of a humanoid that is reaching toward a point. The posture selected depends on the initial posture, the location of the point, and the desired manipulability of the humanoid's arms. A cooperative balancing controller ensures the stability of the reaching motion. In this paper, we propose an algorithm for reaching posture selection and a balancing controller for humanoids, and we present the results of several experiments that confirm the effectiveness of the proposed algorithm and controller.

Keywords Humanoid reaching motion · Balancing controller · Posture selection

1 Introduction

Research is being performed on humanoid walking, running, ladder climbing, manipulating objects, and balancing [1–6]. The purpose of these studies is to enable humanoids to function in dangerous environments such as that caused by the Fukushima nuclear disaster. One expected condition of dangerous environments is that a robot's path will be blocked by obstacles. A humanoid must be able to remove obstacles blocking its path to be able to work in such environments. In this paper, we present an algorithm for motion planning for a humanoid that encounters an obstacle and a balancing controller that addresses stability issues during humanoid motion.

Humanoids are designed to have structural similarities to humans, i.e., two arms and two legs. Given these structural characteristics, a humanoid robot is

Electronic supplementary material The online version of this article (doi:10.1007/s10846-015-0225-z) contains supplementary material, which is available to authorized users.

I. Lee · J.-H. Oh (✉)
Department of Mechanical Engineering,
Korea Advanced Institute of Science and Technology (KAIST), 373-1 Guseong-dong, Yusong-gu,
Daejeon 305-701, Republic of Korea
e-mail: jhoh8@kaist.ac.kr

I. Lee
e-mail: inholee@kaist.ac.kr

able to perform multiple tasks simultaneously. However, this design introduces many degrees of freedom (DOFs) and makes dynamics problems very complicated. In this sense, many humanoids require simpler kinematic approaches. Whole-body inverse kinematic solution, such as task-priority methods, have been developed as a result [7, 8]. These methods require the task Jacobian and its null-space-projection operators. We have found that this approach is suitable for handling the types of multidimensional kinematic problems associated with humanoids. We have applied whole-body inverse kinematics control under joint constraints to the DRC-Hubo humanoid, which was developed in preparation for the DARPA Robotics Challenge (DRC) [9]. The prioritized tasks involved in foot, hand, center-of-mass (COM), and pelvis-related tasks are illustrated in Fig. 1. The pelvis-related tasks include orienting the pelvis attitude and changing the pelvis position. The pelvis-related tasks selected determine the reachability and workspace of the arm. *Inoue* [10] proposed a method for changing the body posture to maximize humanoid arm manipulability. The arm manipulability is a quantitative measure of the arm's ability to position and orient the end-effector. For our purposes, humanoid motion plans are only effective if the humanoid reaches the obstacle in a good position to manipulate it. For that reason, when we select the reaching posture, arm manipulability is considered.

In addition, we would like the humanoid to carry out the performance within a short period of time. Because there are speed limits in each joint, a solution that generates joint trajectories blindly fast is unreasonable. Therefore, we would like to minimize the displacement of joints from the initial posture to the reaching posture. On the other hand, we would like the humanoid to be able to move obstacles blocking its path that may be heavy, and we would like the humanoid to be able to run for extended periods of time. Therefore, the posture of a humanoid while lifting an obstacle should be efficient in terms of energy consumption. Hence, we constructed an optimization problem to select a humanoid posture that maintains high manipulability while minimizing the displacement or energy consumption, as described in Section 2.

Many stability issues arise during the execution of humanoid motions required for reaching, lifting, and releasing. The motions involved in a humanoid reaching for an obstacle are categorized as "reaching" motions, those involved in lifting an obstacle are categorized as "lifting" motions, and those involved in releasing an obstacle from the humanoid's grasp are categorized as "releasing" motions. In reaching motions, external forces act on the end-effector of the humanoid when it makes contact with the obstacle. In lifting and releasing motions, vertical forces act on the end-effector because of the weight of the obstacle. These forces could result in humanoid instability. Previous research on how to compensate for external forces has been conducted by Takubo [11]. Takubo

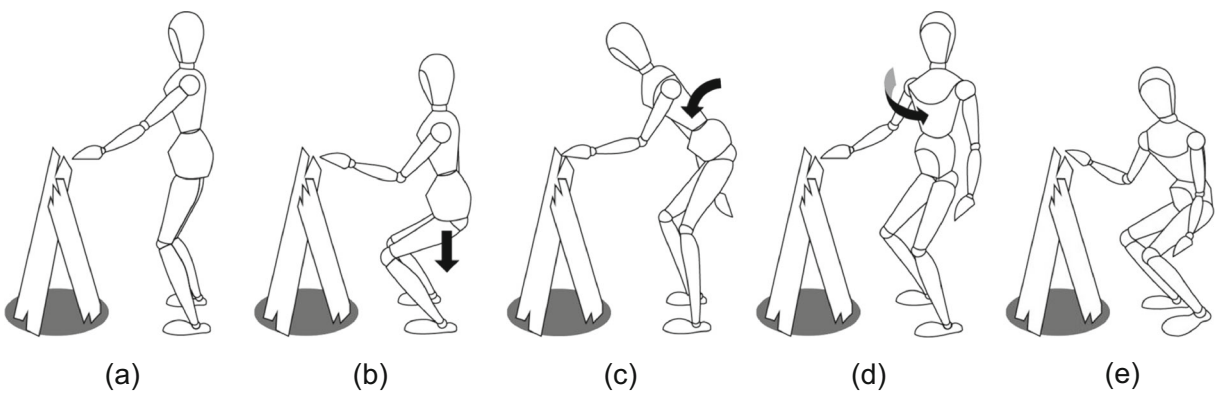

Fig. 1 Sketches of humanoid reaching postures: **a** simply stretched arm posture with low manipulability, **b** motion to lower the height of the pelvis, **c** orienting the pelvis in the pitch direction, **d** orienting the pelvis in the yaw direction, and **e** posture with all motions combined. Pelvis motion increases the manipulability of arms and determines the workspace of the arms

defined the "complement zero-moment point ZMP " (CZMP) as the projection of the COM when external forces act on the end-effectors and proposed modification control of the COM using CZMP to accommodate the external forces. Our proposed balancing controller, described in Section 3, is quite different in that it is able to not only compensate for external forces but also handle the large forces generated when lifting and releasing obstacles. The proposed balancing controller focuses not on locomotion but manipulation such that whole-body motion is controlled. Section 4 presents the results of experiments conducted using the DRC-Hubo that demonstrate the validity of our algorithm for removing obstacles blocking the path of a humanoid.

2 Posture Selection

2.1 Task-Oriented Manipulability and Minimization Matric

The manipulability [12] of robot arms is a quantitative measure of their manipulating ability in positioning and orienting the end-effector. A high degree of manipulability enables a robot to handle obstacles efficiently, whereas a low degree of manipulability makes it difficult to perform such tasks. [13] describes a motion planning algorithm for a mobile manipulator that maintains manipulability by positioning the mobile base. In the case of a humanoid, the position of the shoulder, which is determined by pelvis-related tasks, determines the workspace and reachability of the end-effector. Consequently, pelvis-related tasks are selected to maximize the manipulability of the humanoid arm when reaching for an obstacle. For a given task Jacobian $\dot{x}_a = J_a\dot{\theta}_a$ of the arm, the manipulability MM_a is defined as follows:

$$MM_a = \sqrt{\det(J_a J_a^T)} \tag{2.1}$$

where $x_a = [P_x, P_y, P_z, \omega_x, \omega_y, \omega_z]^T$ is the task of the arm and θ_a is a set of arm joint positions.

We select a posture for a reaching motion that ensures high manipulability and the following minimization matric. One is the displacement of joints, and the other is the energy consumption of the joints. In order to realize a fast and efficient reaching motion, we minimize the displacements of the joints. The angular displacement from the initial posture is defined as follows:

$$D = \sum_i (q_i - q_{0_i})^2 \tag{2.2.1}$$

where q_i is the joint position reference of the humanoid, and q_{0_i} is the joint position of the initial posture.

The energy consumption must also be considered in selecting a reaching posture [14]. The operation of a humanoid over an extended period of time requires that the energy efficiency be taken into account. The energy consumption E_T over a motion time T from the initial posture to the reaching posture is calculated as follows:

$$E_T = \int_0^T \sum_i \tau_i \dot{q}_i dt \tag{2.2.2}$$

where τ_i is the joint torque.

Because pelvis-related tasks determine the reachability, it is important to select the pelvis-related tasks required to perform humanoid reaching motions. There are an uncountable number of solutions for the reaching posture because the pelvis-related tasks introduce additional DOFs for the humanoid. We propose a method for selecting a reaching posture for a humanoid that ensures high manipulability and a minimized angular displacement for pelvis-related tasks or efficient energy consumption.

2.2 Optimization of Posture Selection for Humanoid Reaching Motion

The simplest way to find pelvis-related tasks consists of sampling the tasks within boundaries and repeatedly applying a cost function. However, this requires a high computing power as the number of DOFs for a full humanoid model. For this reason, we simplify a humanoid model for posture selection as shown in Fig. 2a and solve the posture selection problem using an optimization technique.

Figure 2a shows a reaching point T and a position of the shoulder P situated at the origin O, which represents the stance position of a humanoid. The global

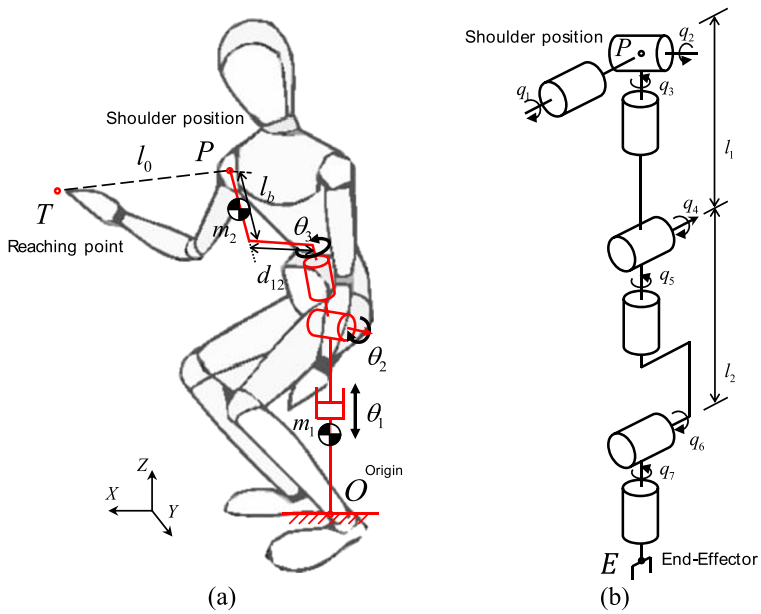

Fig. 2 **a** Simplified kinematic model of pelvis-related tasks and **b** humanoid arm configuration. The simplified kinematic model includes the height of the pelvis, the pitch, and the yaw rotation. The pelvis-related tasks determine the task-oriented manipulability of an arm. We propose an algorithm that optimizes a humanoid posture for a reaching motion, maintaining the high manipulability of the arm

coordinate system is fixed with the origin O at the center of both feet. Figure 2b shows a seven-DOF humanoid arm configuration. This simplified model is applied to right-hand tasks. For left-hand tasks, the direction of the offset d_{12} between the axes of θ_2 and θ_3 is the opposite. The joints of the model are described as follows. The pelvis-related tasks are six-DOF motions that involve a position in three-dimensional Cartesian space and the orientation in a three-dimensional Euclidean space. As shown in Fig. 2a, the simplified humanoid model has a Z position and pitch and yaw orientations. Because the roll orientation has a small compass compared with the pitch and yaw orientations, we can assume that it is zero. In addition, we can assume that the X and Y positions of the pelvis are zero because they are determined passively to fix the COM. For that reason, in Fig. 2a, the position P of the shoulder is different. However, the difference is small because the weight of the arm is relatively small in most humanoids. The issue of stability is discussed in the next section. We assumed that the difference in the position of the shoulder is zero. Eventually, to plan a reaching motion by the humanoid, we select three pelvis DOFs: the height of the pelvis and the pitch and yaw orientations of the pelvis. θ_1 is described by a angular displacement of the pelvis height, and θ_2 and θ_3 are described by angular displacements of the pitch and yaw orientations. We select a humanoid posture for reaching with a minimized displacement of the pelvis-related tasks or energy consumption. The following statements describe the case when minimizing the displacement of the pelvis-related tasks, and we describe in case when minimizing the energy consumption in Section 2.3.

The distance l_0 between the reaching point T and the shoulder position P, which is the length of the humanoid's arm, is a dominant parameter in the arm manipulability MM_a. As mentioned above, a high degree of arm manipulability is required to enable the robot to handle obstacles efficiently. Figure 3 shows examples of manipulability distributions calculated as functions of the distance between the base (shoulder position) and the end-effector.

Conversely, we can construct a database g of distances l_0 depending on the desired manipulability MM_{des}.

$$g(q_1, q_2, q_3, q_4, q_5, q_6, q_7, MM_{des}) \approx l_0^2 \tag{2.3}$$

The shoulder position P^O with respect to the origin O is obtained from the transformation matrix T_P^O:

$$T_P^O = Trans_{z,\theta_1} R_{Y,\theta_2} R_{Z,\theta_3} Trans_{Y,d_{12}} Trans_{Z,l_b} \tag{2.4}$$

$$T_P^O = \begin{bmatrix} R_P^O & P^O \\ 0 & 1 \end{bmatrix} \tag{2.5}$$

As a result, the shoulder position $P^O \in \mathrm{R}^3$ is calculated as follows:

$$P_x^O = l_b \sin(\theta_2) - d_{12} \cos(\theta_2) \sin(\theta_3) \tag{2.6.1}$$

$$P_y^O = d_{12} \cos(\theta_3) \tag{2.6.2}$$

$$P_z^O = \theta_1 + \theta_{0_1} + l_b \cos(\theta_2) + d_{12} \sin(\theta_2) \sin(\theta_3) \tag{2.6.3}$$

From Eq. 2.2.1, the displacements of the joints are associated with the three pelvis-related tasks. Therefore an optimization problem for minimizing the displacements of the joints moving from the initial posture to a reaching posture with equality constraints can be expressed as follows:

$$\min \quad f(\theta_1, \theta_2, \theta_3)$$

$$s.t. \quad g(\theta_1, \theta_2, \theta_3)$$

where

- The minimization equation for the displacement of pelvis-related tasks from the initial posture Θ_0 to the reaching posture $\Theta = (\theta_1, \theta_2, \theta_3)$ is expressed as:

$$f(\theta_1, \theta_2, \theta_3) = \|\Theta - \Theta_0\|^2 \tag{2.7.1}$$

- The equality constraint is obtained by using Eq. 2.3 to construct the equality constraints for minimization is:

$$g(\theta_1, \theta_2, \theta_3) = \left\| T^O - P^O \right\|^2 - l_0^2 = 0, \text{ where } P^O \in \mathrm{R}^3 \text{ and } T^O \in \mathrm{R}^3 \tag{2.7.2}$$

To solve this minimization problem, we introduce a new variable λ, called a Lagrange multiplier, and we examine the Lagrange function, defined as follows:

$$\Lambda(\theta_1, \theta_2, \theta_3, \lambda) = f(\theta_1, \theta_2, \theta_3) + \lambda \cdot g(\theta_1, \theta_2, \theta_3) \tag{2.8.1}$$

$$\nabla \Lambda = \nabla f + \lambda \nabla g = 0 \tag{2.8.2}$$

and we solve for θ_1, θ_2 and θ_3 for each pelvis task.

$$\frac{\partial f}{\partial \theta_i}(\theta_1, \theta_2, \theta_3) - \lambda \cdot \frac{\partial g}{\partial \theta_i}(\theta_1, \theta_2, \theta_3) = h_i(\theta_1, \theta_2, \theta_3, \lambda) = 0 \tag{2.9.1}$$

$$g(\theta_1, \theta_2, \theta_3) = h_4(\theta_1, \theta_2, \theta_3, \lambda) = 0 \tag{2.9.2}$$

Thus, a solution set of the optimization problem is defined by the four simultaneous equations expressed as Eq. 2.9.1 and Eq. 2.9.2. However, as shown in Eqs. 2.6.1 to 2.6.3, it is difficult to solve these simultaneous equations because they are complicated and nonlinear. Therefore, we solved the simultaneous equations using the Levenberg–Marquardt (LM) algorithm, which is an iterative technique that locates the minimum of a multivariable function that is expressed as the sum of squares of nonlinear real-valued functions [15, 16]. A parameter vector set Q of the LM algorithm is $[\theta_1, \theta_2, \theta_3, \lambda]^T$, and an estimated measurement vector X is $[0, 0, 0, 0]^T$. This algorithm seeks to find the vector Q_f that best satisfies the functional relational functions h_i, i.e., those minimize the squared distance $Q_e^T Q_e$ given $Q_e = X - \hat{X}$. The term

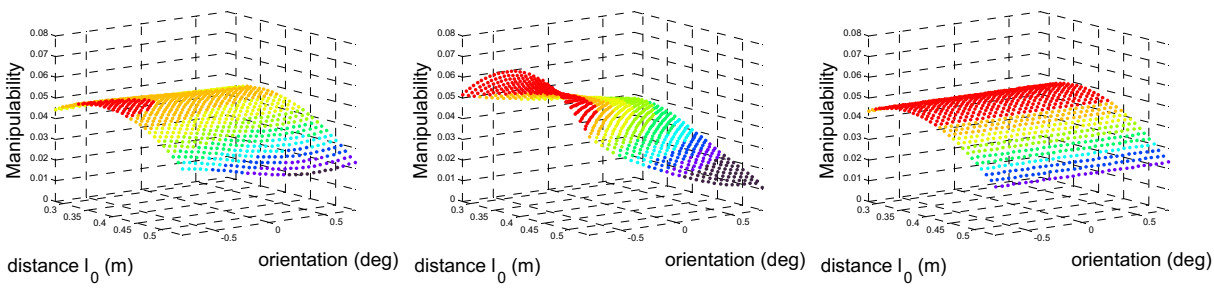

Fig. 3 A distribution map of the manipulability and distance ; the distance is from 0.30m to 0.55m , and the end-effecter orientation ranges from -60° to 60° in the **a** X direction, **b** Y direction, and **c** Z direction. When the position and orientation for the humanoid reaching point is determined, these distribution maps of manipulability determine the distance between the shoulder and the end-effecter according to the desired arm manipulability

Fig. 4 Pseudo code for the proposed posture selection algorithm

Input := A target position $T \in \mathbb{R}^3$, a desired manipulability of arm MM_a and a initial posture Θ_0 where $\Theta = \theta_1 + \theta_2 + \theta_3$.
Output := A vector of pelvis-related tasks $\Theta \in \mathbb{R}^3$ minimizing $f(\Theta) = \|\Theta - \Theta_0\|^2$.
Algorithm :=

$P := A\,shoulder\,position\,P \in \mathbb{R}^3$
$g(\Theta) := \|T - P\|^2 - l_0^2;$
$Q := [\theta_1\ \theta_2\ \theta_3\ \lambda]^T;$
$X := [X_1\ X_2\ X_3\ X_4]^T = h(Q);$
  $X_1 := \partial f(\Theta)/\partial\theta_1 - \lambda \cdot g(\Theta)/\partial\theta_1 := h_1(Q);$
  $X_2 := \partial f(\Theta)/\partial\theta_2 - \lambda \cdot g(\Theta)/\partial\theta_2 := h_2(Q);$
  $X_3 := \partial f(\Theta)/\partial\theta_3 - \lambda \cdot g(\Theta)/\partial\theta_3 := h_3(Q);$
$Q_e := [0\,0\,0\,0]^T - X := -h(Q);$
$H := J^T W_E J + W_N;$
$H_{inv} := inv(H);$
$Q_{LM} := H_{inv} J^T W_E Q_e;$
$k := 1;$

$while(not\ stop)\ and\ (k < N_{\max})$
  $k := k + 1;$
  $repeat$
    $if\ (\|Q_e\| \le \varepsilon)\ //\ convergence\,test..(percentage\,test)$
      $stop := true;$
    $else$
      $Q := Q + Q_{LM};$
    $endif$
  $until(stop)$
$endwhile$

$\hat{X}$ is the result of the functional relational functions h_i for the vector set Q. A linear approximation to h in the neighborhood of Q is defined as follows:

$$Q_{k+1} = Q_k + J_k Q_e \tag{2.10}$$

By applying a damping matrix to the LM algorithm, the Jacobian matrix J_k is redefined as follows:

$$\begin{aligned} Q_{k+1} &= Q_k + (J_k^T W_E J_k + W_N)^{-1} g_k, \text{ where} \\ g_k &= J_k^T W_E Q_e \end{aligned} \tag{2.11}$$

This numerical iteration minimizes the following equation for the squared distance $Q_e^T Q_e$.

$$E(Q) = \frac{1}{2} Q_e^T W_E Q_e \to \min \tag{2.12}$$

The pseudo code for our proposed posture selection algorithm is shown in Fig. 4. The algorithm seeks the values of the three pelvis-related task position parameters that ensure the desired manipulability while minimizing energy consumption.

2.3 Minimization of the Energy Consumption and Humanoid Motion Generation

From Eqs. 2.7.1 to 2.12, we select the pelvis-related tasks for the reaching motion to ensure high manipulability while minimizing the joint displacement. The following statements describe the posture selection when minimizing the joint energy consumption. Using Eq. 2.2.2, the minimization equation for the energy consumption from the initial posture to the reaching posture is derived as

$$E_T = \int_0^T \sum_{i=1}^{3} \tau_i \dot{\theta}_i dt \tag{2.13}$$

where τ_i is the joint torque, and T is the reaching motion time. The joint torques are associated with the posture $\theta_1, \theta_2, \theta_3$ and the accelerations of the masses m_1, m_2. The torque equations are very complicated and require considerable computing power; therefore, we simplify these torque equations with the simpler

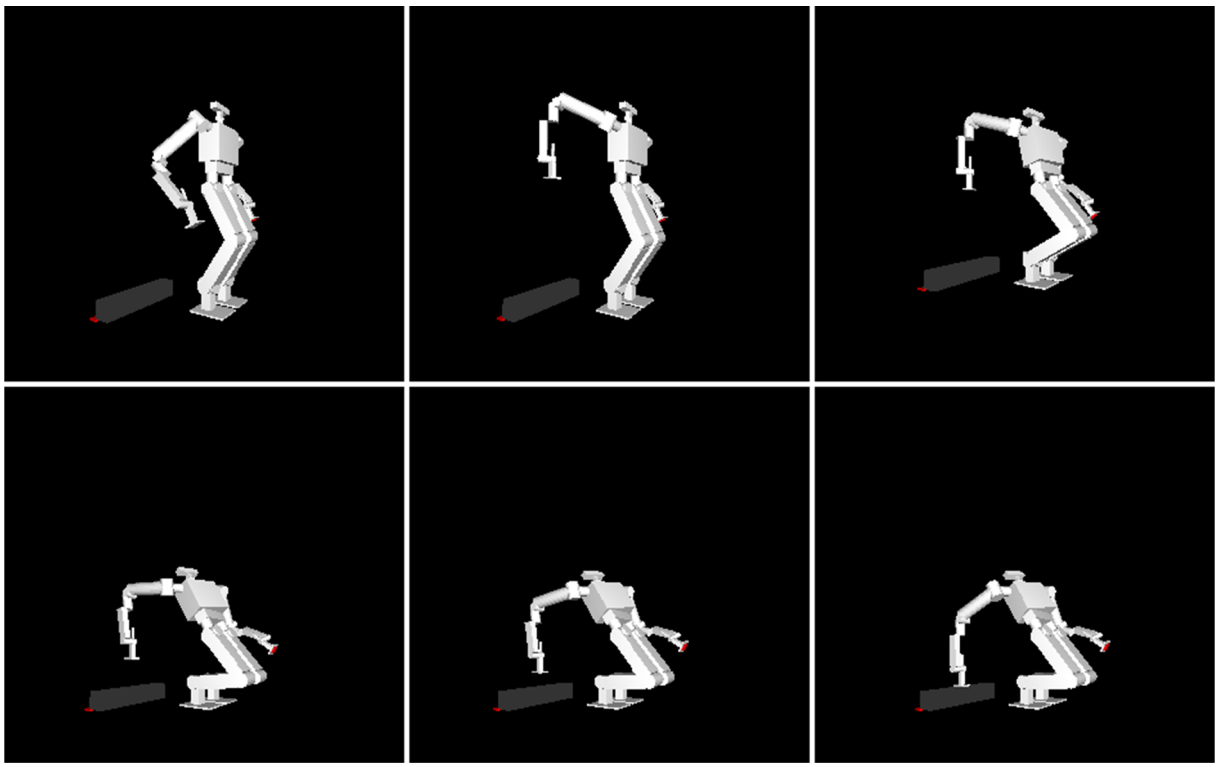

Fig. 5 Selected humanoid reaching posture. Because of humanoid kneeling direction, the humanoid reaches the target backwards. This figure shows that the humanoid reaching motion is backwards . In order to remove an obstacle in the movement path, the humanoid reaches the obstacle with a reaching posture selected by our posture selection algorithm

kinematic torque equations r_i. The simplified torque equations are only associated with the posture.

$$E_T \simeq \int_0^T \sum_{i=1}^{3} r_i(\theta_1, \theta_2, \theta_3)\dot{\theta}_i dt \tag{2.14}$$

To solve the minimization problem in Fig. 4, we should obtain the energy consumption exactly. Therefore, we calculate Eq. 2.14 with a finite numerical integration:

$$E_T \simeq \sum_{k=0}^{N} \sum_{i=1}^{3} r_i(\theta_{1k}, \theta_{2k}, \theta_{3k}) \frac{\theta_i}{N} \frac{T}{N} \tag{2.15}$$

where the trajectories of θ_i are assumed to be simple ramp functions. Finally, we derive a new minimization equation and substitute Eq. 2.7.1. Then, we repeat the above process to solve the minimization problem and select the reaching posture.

Figure 5 shows a humanoid posture that reaches the target point [−0.40 −0.25 0.10]. The figure illustrates the manipulability of the humanoid arm from the initial posture to the final posture.

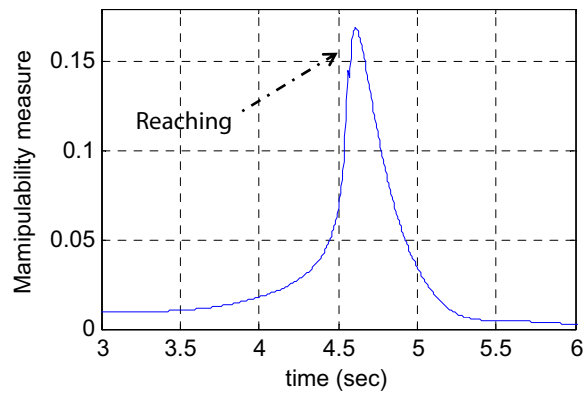

Fig. 6 Manipulability measure of humanoid arm during the reaching motion shown in Fig. 5. The arm manipulability is high at the reaching time. The reaching posture at that time is shown in the last snap shot in Fig. 5

To establish the relative priorities as part of the overall performance expectations for our proposed posture selection algorithm, we can assign weighting factors ($W_S = [W_{S1}\ W_{S2}\ W_{S3}]^T$) to Eq. 2.7.1, as shown in Eq. 2.17. If we want to obtain a posture with a small change in one pelvis-related task, we increase the weighting factor for that task. For example, by increasing the weighting factor for the yaw orientation θ_3, pelvis-related tasks are excluded. This technique can be applied to posture selection to handle obstacles with two hands. Figure 7b shows the result for two hands reaching a target obtained using the modified minimization equation Eq. 2.17 .

$$f(\theta_1, \theta_2, \theta_3) = (\theta_1 - \theta_{0_1})^2 + (\theta_2 - \theta_{0_2})^2 + (\theta_3 - \theta_{0_3})^2 \quad (2.16)$$

$$\begin{aligned} f(\theta_1, \theta_2, \theta_3) &= W_S \cdot \|\Theta - \Theta_0\|^2 \\ &= W_{S1} \cdot (\theta_1 - \theta_{0_1})^2 + W_{S2} \cdot (\theta_2 - \theta_{0_2})^2 \\ &\quad + W_{S3} \cdot (\theta_3 - \theta_{0_3})^2 \end{aligned} \quad (2.17)$$

As shown in Fig. 7a, there is a twist angle in the Z direction of the upper body that resembles the reaching posture shown in Fig. 5. On the other hand, there is no twist angle in Fig. 7b because we selected a weight factor W_{S3} that is much higher than the others for this term. As the reaching posture in Fig. 7c shows, the posture can be applied to the situation of a humanoid reaching an obstacle with two hands.

3 Cooperative Balancing Controller

3.1 Inverted Pendulum Model with a Compliant Joint

Collisions can occur when humanoids reach for obstacles. Such collisions represent situations in which external forces are applied to a humanoid. In addition, when a humanoid lifts an obstacle with a weight in the range of approximately 1 to 5 kg, vertical forces are applied to the hand. Lastly, discontinuous forces occur when the obstacle is released. Thus, humanoid motion introduces instability issues. A balance controller is therefore required to ensure stability during humanoid motions when removing obstacles.

Our balancing controller uses an inverted pendulum model with a compliant joint, as illustrated in Fig. 8. The high-gain proportional and derivative (PD)-controlled position-based robot Hubo usually uses an inverted pendulum with a compliant joint model [17]. These models have high stiffness and low damping characteristics. Consequently, when external forces are applied, an oscillation occurs at a high frequency. Moreover, a high gain cannot be used to regulate the ZMP when we design a ZMP compensator because an inverted pendulum system with a compliant joint is considered to be a near-non-minimum phase system, and the two poles of the system are near the imaginary axis, as shown in Fig. 9. Therefore, we improve the damping characteristics through the use of a balance controller.

The linearized equation of motion of the system is as follows:

$$ml^2\ddot{\theta} = \tau - b\dot{\theta} - mgl\theta \quad (3.1)$$

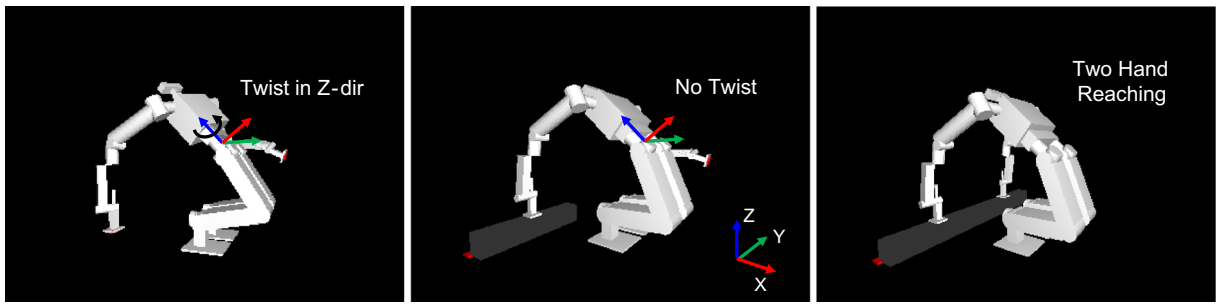

Fig. 7 Selected humanoid posture excluding the yaw orientation of pelvis-related tasks. By selecting a weighting factor, we can regulate the pelvis-yaw rotation. In addition, the selected posture is used for a two-hand reaching motion

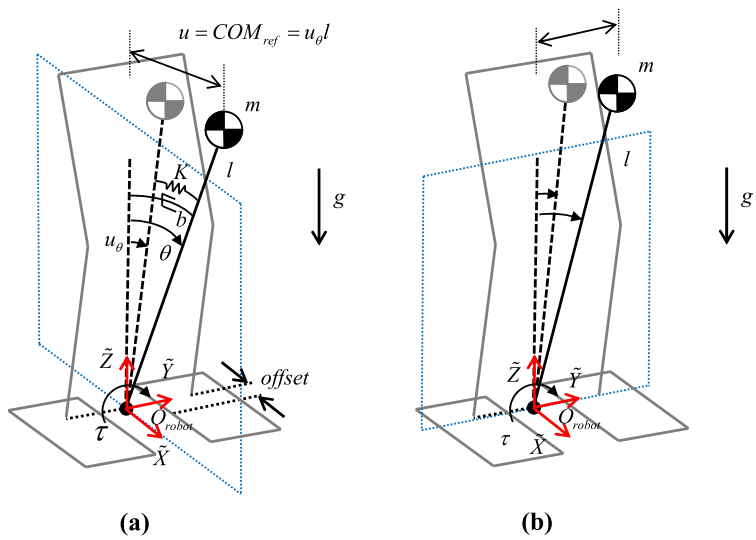

Fig. 8 Inverted pendulum model with a compliant joint defined in **a** the sagittal plane and **b** the lateral plane. We conduct a frequency response test in order to identify the unknown compliant values

In this equation, m is the mass of the pendulum; l is the length of the pendulum; θ is the inclined angle due to compliance; τ is the external torque acting on the system, $\tau = -K(\theta - u_\theta)$; u_θ is the reference angle derived from the reference position of the COM (u, $u_\theta = u/l$); and K and b are the stiffness and damping coefficients, respectively, pertaining to the compliance. We define a state vector as $x = [\theta\ \dot{\theta}]^T$ and the ZMP as the output of the system. The system equation is obtained from the equations below.

$$\frac{d}{dt}x = \begin{bmatrix} 0 & 1 \\ \frac{g}{l} - \frac{K}{ml^2} & -\frac{b}{ml^2} \end{bmatrix} x + \begin{bmatrix} 0 \\ \frac{K}{ml^2} \end{bmatrix} u_\theta$$
$$y = ZMP = \begin{bmatrix} \frac{K}{mg} & \frac{b}{mg} \end{bmatrix} x + \begin{bmatrix} -\frac{K}{mg} \end{bmatrix} u_\theta \tag{3.2}$$

In experiments conducted using a real robot, the COM control input is determined in real time using the measurement equation given below and the force/torque sensor attached to the foot. The measured ZMP is given as follows:

$$\begin{bmatrix} \tilde{x}_{ZMP} \\ \tilde{y}_{ZMP} \end{bmatrix} = \frac{1}{f_{RF_Z} + f_{LF_Z}} \begin{bmatrix} -\tau_{\tilde{y}} \\ \tau_{\tilde{x}} \end{bmatrix}$$
$$= \overrightarrow{\tau}_{RF} + \overrightarrow{\tau}_{LF} + \overrightarrow{OP}_{RF} \times \overrightarrow{f}_{RF_Z} + \overrightarrow{OP}_{LF} \times \overrightarrow{f}_{LF_Z} \tag{3.3}$$

where $\overrightarrow{f}_{RF_Z}$ and $\overrightarrow{f}_{LF_Z}$ are the measured normal forces and $\overrightarrow{\tau}_{RF}$ and $\overrightarrow{\tau}_{LF}$ are the measured torques on the right foot and left foot, respectively, and $\overrightarrow{OP}_{RF}$ and $\overrightarrow{OP}_{LF}$ are the position vectors of the right foot and left foot, respectively, in Cartesian coordinates.

3.2 System Identification and Pole Placements

The input to the transfer function is the COM position, and the output is the ZMP. Using frequency

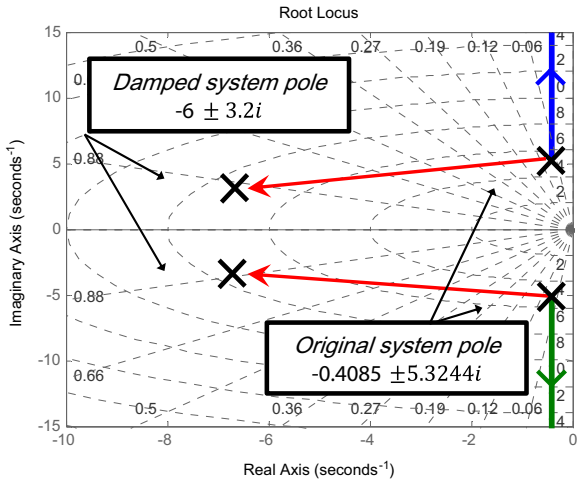

Fig. 9 Pole placement for the improved damped system. Because the second-order dynamic model has two poles located near the imaginary axis, we place the poles on the left side in order to make the system damped

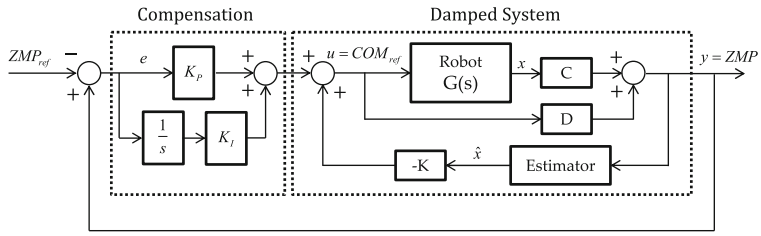

Fig. 10 Block diagram of the proposed balancing controller including the damping controller and ZMP compensator. In order to balance itself, a humanoid should maintain the ZMP on one foot. Because the system is close to a non-minimum system, the simply selected ZMP compensator gain could excite the system. Therefore, we place the poles at improved damped pole location, and the damped system makes the system robust against discontinuous external forces

response methods, the following transfer function for the system is obtained:

$$\frac{ZMP}{u_\theta} = \frac{-\frac{K}{mg}(s^2 + \frac{g}{l})}{s^2 + \frac{b}{ml^2}s + \frac{g}{l} + \frac{K}{ml^2}} = \frac{a}{s^2 + 2\xi\omega_n s + \omega_n^2} \tag{3.4}$$

where $a = 38.33$, $\omega_n = 5.342$, and $\xi = 0.07649$

Figure 9 shows the root locus of the original system and the damped system. The two poles of the original system are placed on the desired pole using a pole placement method. The control input is determined by multiplying the state feedback gain K by the estimated state $\hat{x}$, as shown in Fig. 10.

A block diagram of the proposed controller is shown in Fig. 10. The proposed balancing controller includes a ZMP compensator and damped system. The ZMP compensator regulates the ZMP with respect to a reference value of zero with PI (proportional position and integral action) compensation in response to the external forces generated by collision and the weight of the obstacle. The PI gain is selected using a heuristic process.

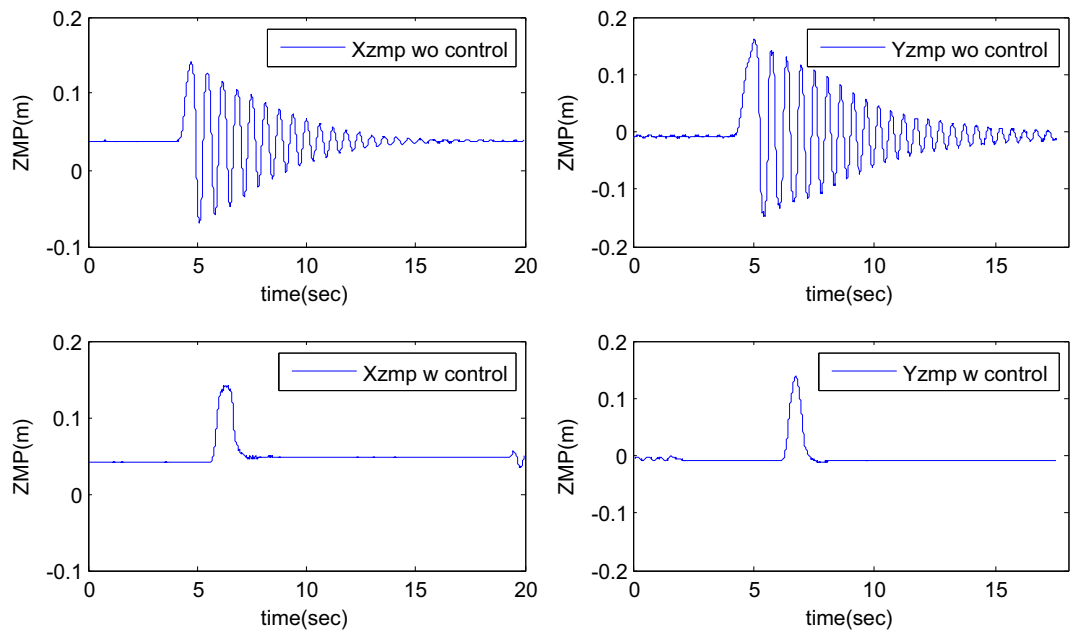

Fig. 11 ZMP results of experiment for improved damped system. This ZMP graph shows the validity of the improved damped system. The oscillation is removed by the pole-placement

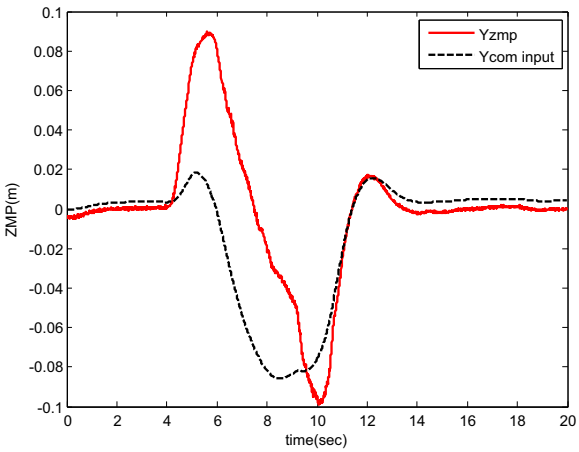

Fig. 12 Measured ZMP in the Y direction during an experiment in which external forces are applied to the humanoid. The designed ZMP compensator maintains the ZMP of the humanoid on one foot against external forces

3.3 Effectiveness of the Damping Controller and ZMP Compensator

Figures 11 and 12 show the results for the balancing controller in the experiments. Figure 11 shows the measured ZMP of the humanoid robot in the X and Y directions. We applied external forces to the humanoid robot to shift its posture. For an uncontrolled system, the shifted ZMP decreases with high-frequency vibration. On the other hand, the shifted ZMP converges toward a steady state with a minor oscillation resulting from the improved damping characteristics. On the basis of these results, we expect the system to be stable when the humanoid hand comes into contact with an obstacle or the environment and when it releases the obstacle.

Figure 12 shows the ZMP results from experiments in which external forces are applied to the humanoid. The experiments verify the effectiveness of the PI compensator as a balancing controller. The PI compensator prevents instability during the lifting of a heavy obstacle. The COM control input is generated by external forces and stabilizes the system against unknown forces. The converged ZMP demonstrates that our system successfully stabilizes after an external force is applied. Therefore, we expect the system to be stable when the humanoid lifts an obstacle of unknown weight.

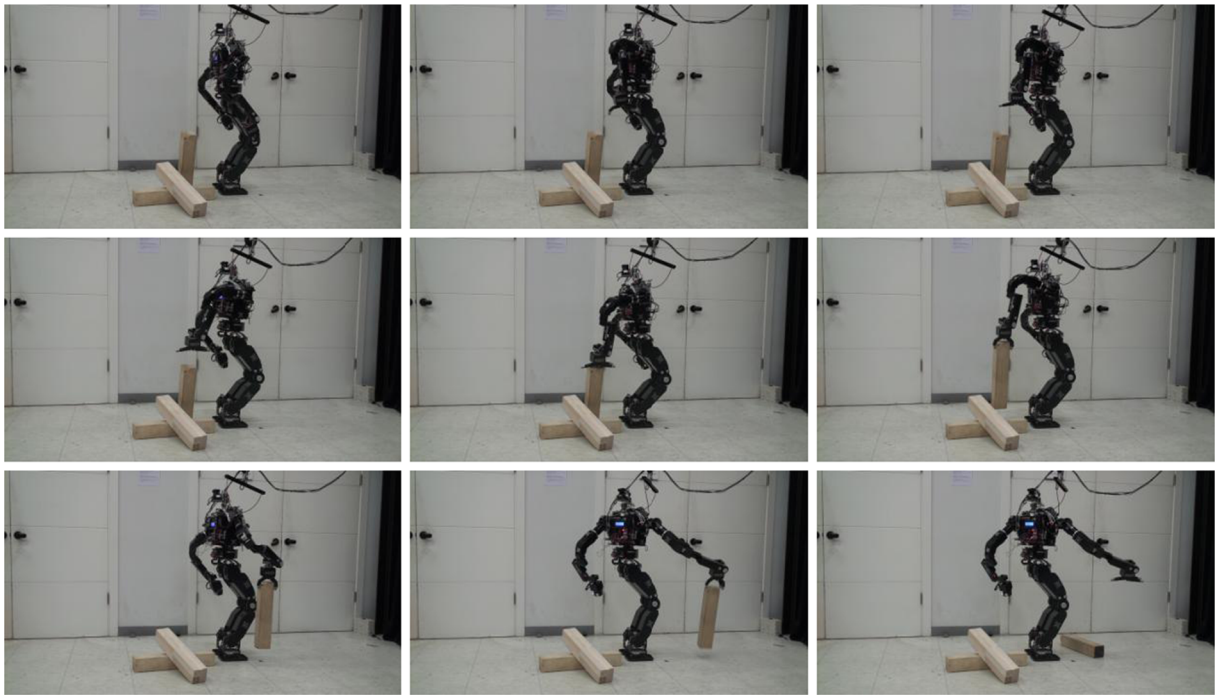

Fig. 13 Photographs of the removal motions for the first obstacle. Photographs of the removal motions for the additional obstacles are shown in the Appendices

4 Experiments

4.1 Obstacles Removal Motion Generation for a Humanoid

In the experiment described below, the humanoid robot was required to remove obstacles that were blocking its way. As with the many motions demonstrated earlier, the removal motions are generated backwards because the humanoid is designed to bend inward. In the experiment, three obstacles lay randomly within the movement path of the humanoid. The reaching point was determined by an operator. The reaching posture was selected using our proposed method. The reaching motion was generated by a simple sinusoidal function using the proposed cooperative balancing controller. Figure 13 shows the first obstacle removal motion performed by the robot. Photo graphs of the second and third removal motions are shown in the Fig. 14.

4.2 Effectiveness of Cooperative Balancing Controller during Motion

We conducted several experiments with a robot to assess the performance of the proposed balancing controller during obstacle removal. The experimental environment was constructed as shown in Fig. 15a. The humanoid was expected to remove debris in its movement path, which was bordered by brick walls. Figures 15b and 15c show the measured ZMP and vertical force applied to the wrist.

In Fig. 15, the left hand reached the obstacle after 12 s. As shown in Figure (c), the reaction force on the left wrist increased. Until the robot grasped the debris correctly, unknown external forces were applied to the left hand because of the grasping power. The ZMP of the robot initially moved forward. Eventually, the ZMP converged by means of PI compensation. At 27 s, the robot had lifted the debris completely. While the robot was lifting the obstacle, the ZMP compensator

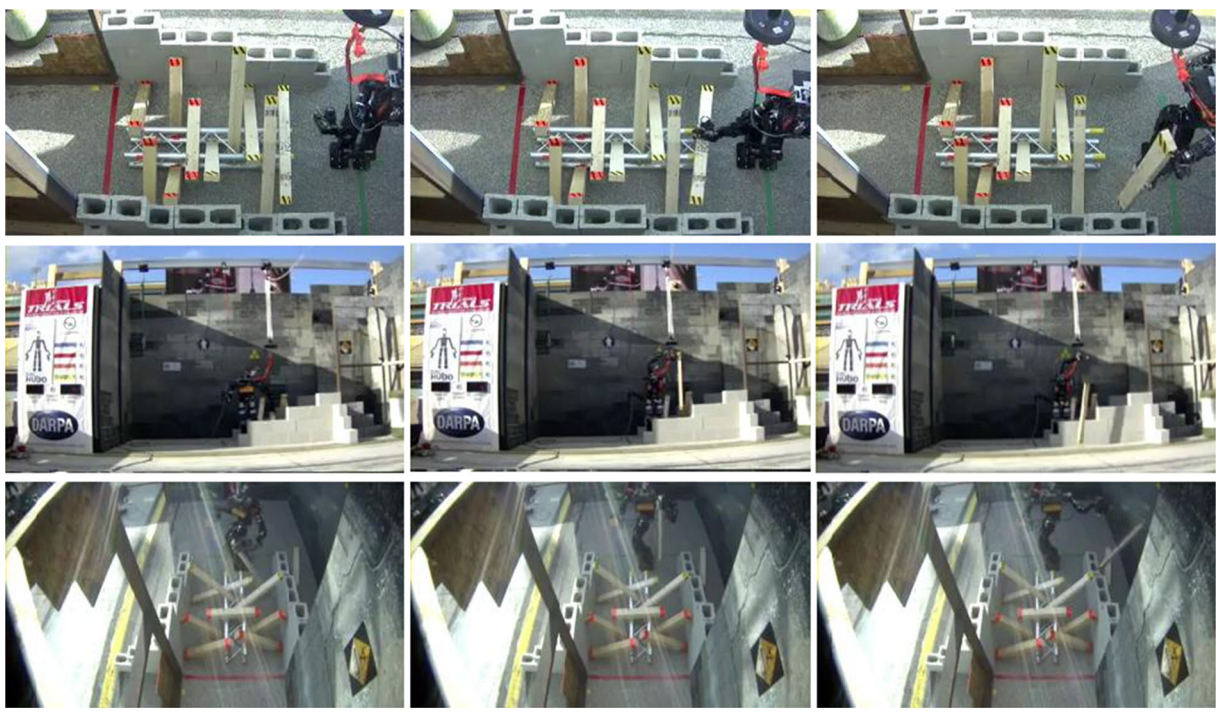

Fig. 14 Photographs of obstacle removal motion in the 2013 DARPA Robotics Challenge Trials in which the humanoid DRC-Hubo participated. The humanoid's performance is illustrated in this figure. The sixth and ninth scenes show debris lifted and removed from the brick wall

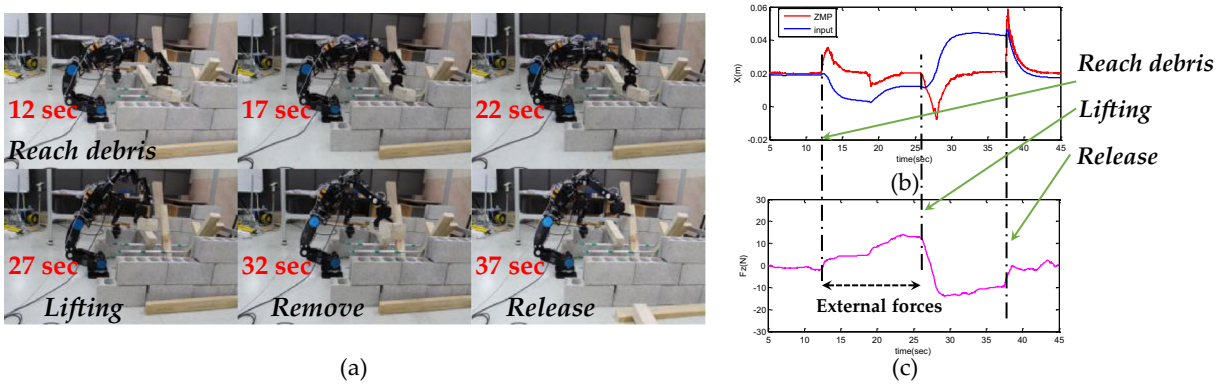

Fig. 15 Experiment conducted with a real robot. **a** Photographs taken during an obstacle removal experiment, **b** measured ZMP and controller input, **c** applied vertical force on the wrist sensor

of our proposed balancing controller regulated the external forces associated with the obstacle weight. The robot moved the debris to an area outside the wall within 36 s. At 37 s, the debris was released, which we were able to confirm because the measured force value decreased. At that time, the ZMP moved forward instantly because of the change in the hand weight. The effectiveness of the improved damping characteristics provided by the proposed controller helped to reduce vibration in the system, and the ZMP converged by means of the ZMP compensator. As a result, we were able to verify that the proposed cooperative balancing controller maintained the stability of the system.

5 Discussion

In this paper, we present a motion planning algorithm for a humanoid for use in removing obstacles blocking the humanoid's path. The motion planning algorithm includes posture selection for reaching objects and a cooperative balancing controller for stabilizing the humanoid.

The reaching posture of the humanoid is selected in two ways. They are solved an optimization problem to ensure high manipulability of the arm while minimizing task displacement from initial posture and minimizing energy consumption. The optimization problem is constrained by the arm length, which determines the manipulability of the arm. The arm length constraint is determined by selecting a desired manipulability that is sufficiently high to enable the robot to efficiently handle the object.

The cooperative balance controller simplifies the humanoid as an inverted pendulum with a compliant joint model. This system improves the damping characteristics of the humanoid and regulates its external force using a PI compensator. Experiments conducted using a robot demonstrate the validity of this system. The balance controller can be applied to high-gain PD-controlled position-based humanoid robots.

6 Conclusion and Recommendation

While the proposed motion planning algorithm brings humanoids one step closer to being able to clear obstacles autonomous ly in disaster environments, there are still many relevant research problems that must first be addressed. In the proposed motion planning algorithm, the position of the grasping point on the obstacle is determined by the operator. A recognition algorithm with the ability to identify removable obstacles and determine the positions of grasping points is required to develop a fully autonomous system. In addition, many disaster situations require that the debris be carried some distance, while our framework only applies to situations in which the humanoid's feet are firmly planted. Locomotion strategies must be developed for the humanoid to be able to carry obstacles to desired locations.

Appendix:

The preparation video of TEAM KAIST is uploaded on following URL:
https://www.youtube.com/watch?v=Dd3pMeAnl8c.

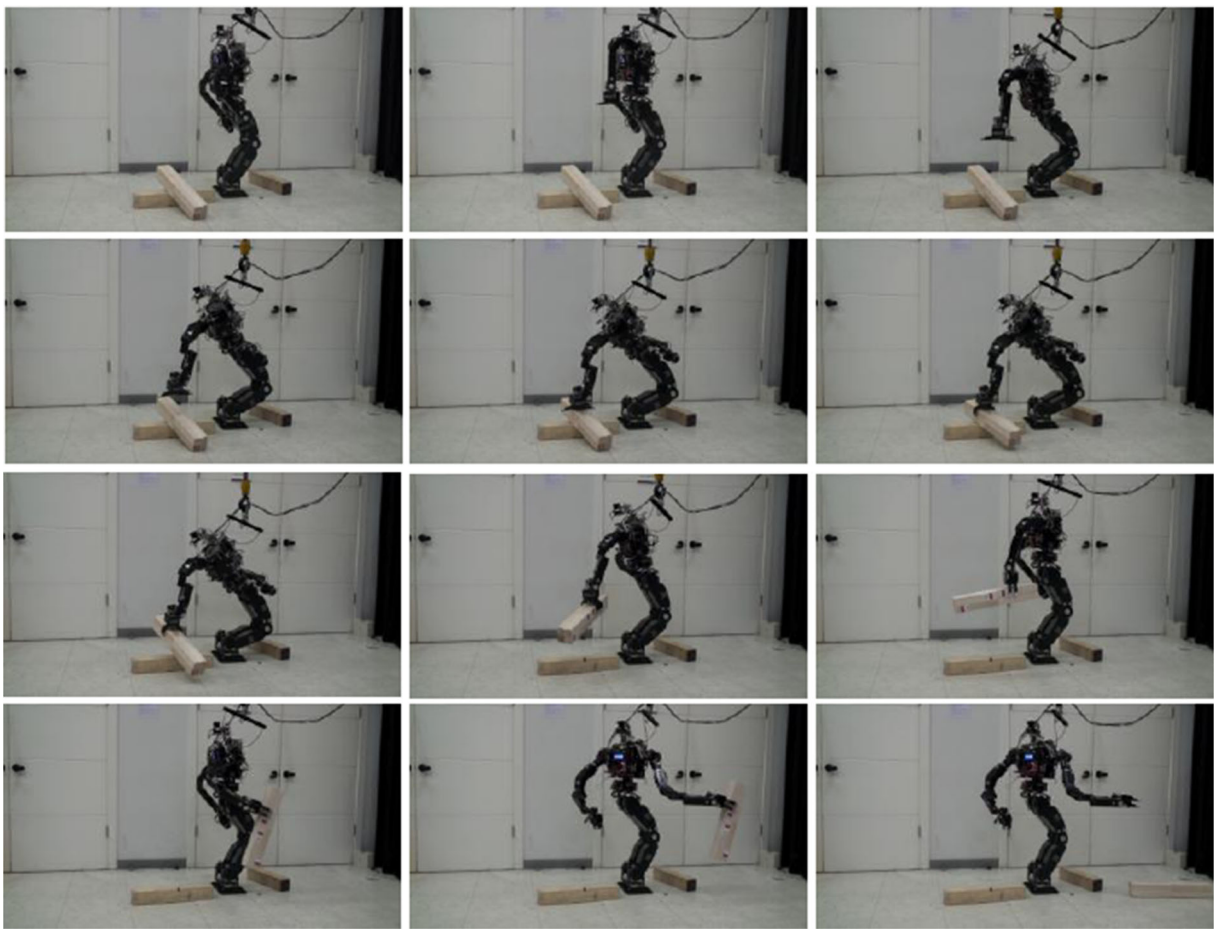

Fig. 16 Photographs of motions for the removal of the second obstacle

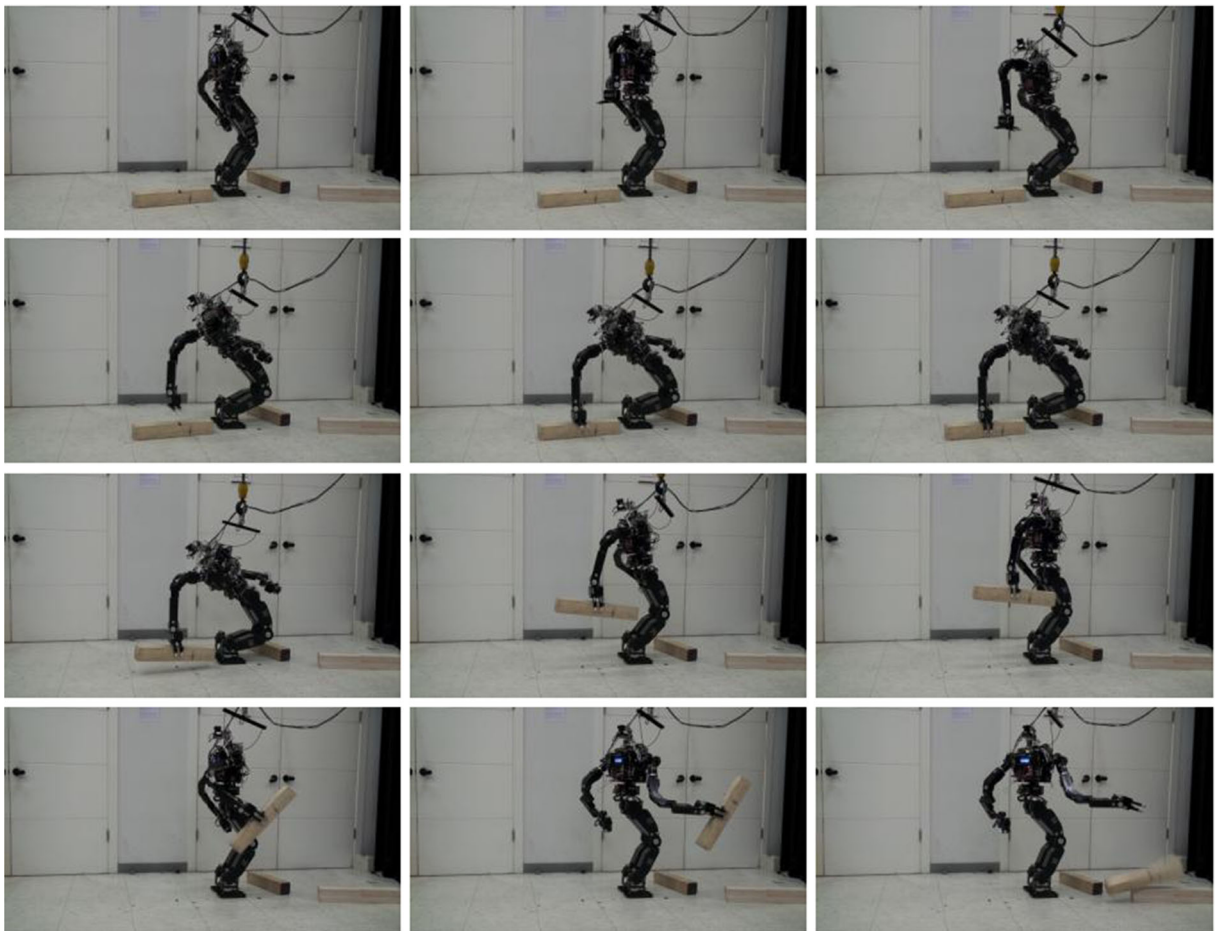

Fig. 17 Photographs of motions for the removal of the second obstacle

References

1. Kajita, S., et al.: Biped walking stabilization based on linear inverted pendulum tracking. In: IEEE/RSJ International Conference on Intelligent Robots and Systems (IROS). IEEE (2010)
2. Kajita, S., et al.: Biped walking pattern generation by using preview control of zero-moment point. In: Proceedings of the IEEE International Conference on Robotics and Automation, ICRA'03, vol. 2. IEEE (2003)
3. Kajita, S., et al.: A running controller of humanoid biped HRP-2LR. In: Proceedings of the 2005 IEEE International Conference on Robotics and Automation, ICRA 2005. IEEE (2005)
4. Yoneda, H., et al.: "Vertical ladder climbing motion with posture control for multi-locomotion robot". In: IEEE/RSJ International Conference on Intelligent Robots and Systems, IROS 2008. IEEE (2008)
5. Ott, C., et al.: A humanoid two-arm system for dexterous manipulation. In: 6th IEEE-RAS International Conference on Humanoid Robots, 2006. IEEE (2006)
6. Kim, M.-S., Oh, J.H.: Posture control of a humanoid robot with a compliant ankle joint. Int. J. Humanoid Robot. **7.01**, 5–29 (2010)
7. Nakamura, Y., Hanafusa, H., Yoshikawa, T.: Task-priority based redundancy control of robot manipulators. Int. J. Robot. Res. **6.2**, 3–15 (1987)
8. Kanoun, O., Lamiraux, F., Wieber, P.-B.: Kinematic control of redundant manipulators: Generalizing the task-priority framework to inequality task. IEEE Trans. Robot. **27.4**, 785–792 (2011)
9. Kim, I., Oh, J.-H.: Inverse kinematic control of humanoids under joint constraints. Int. J. Adv. Robot. Sy. **10**, 74 (2013)
10. Inoue, K., et al.: Mobile manipulation of humanoid robots-body and leg control for dual arm manipulation. In: Proceedings of the IEEE International Conference on Robotics and Automation, 2002, ICRA'02, vol. 3. IEEE (2002)
11. Takubo, T., et al.: Mobile manipulation of humanoid robots-control method for com position with external force. In: Proceedings of the IEEE/RSJ International Conference on Intelligent Robots and Systems, 2004, (IROS 2004), vol. 2. IEEE (2004)

12. Yoshikawa, T.: Dynamic manipulability of robot manipulators. In: Proceedings of the IEEE International Conference on Robotics and Automation, vol. 2. IEEE (1985)
13. Nagatani, K., et al.: Motion planning for mobile manipulator with keeping manipulability. In: IEEE/RSJ International Conference on Intelligent Robots and Systems, 2002, vol. 2. IEEE (2002)
14. Zhang, Y., Ma, S.: Minimum-energy redundancy resolution of robot manipulators unified by quadratic programming and its online solution. In: International Conference on Mechatronics and Automation, ICMA 2007. IEEE (2007)
15. Levemberg, K.: A method for the solution of certain problems nonlinear in least square. Quarth. Appl. Math. **2**, 164–168 (1944)
16. Marquardt, D.W.: An algorithm for least-squares estimation of nonlinear parameters. J. Soc. Ind. Appl. Math. **11.2**, 431–441 (1963)
17. Park, I.-W., Kim, J.-Y., Oh, J.-H.: Online walking pattern generation and its application to a biped humanoid robot–KHR-3 (HUBO). Adv. Robot. **2–3**, 159–190 (2008)

Inho Lee received his B.S. degree in Mechanical Engineering from Korea Advanced Institute of Science and Technology (KAIST), Daejeon, South Korea, and M.S. in Mechanical Engineering from KAIST, in 2009 and 2011, respectively. Since 2011, he is currently pursuing the Ph.D. degree in Mechanical engineering at the KAIST and working on the project of development for humanoid robots: HUBO, HUBO2 and DRC-HUBO. His research interests include motion planning, quadruped and bipedal walking and stabilization control for a humanoid robot, biomechanics, sensors, actuators and application of micro-processor.

Jun-Ho Oh received his B.S. and M.S. degrees in Mechanical Engineering from Yonsei University, Seoul, South Korea, and has Ph.D. degree in Mechanical Engineering from University of California, Berkeley, in 1977, 1979, and 1985 respectively. He was a Researcher with the Korea Atomic Energy Research Institute, from 1979 to 1981. Since 1985, he has been with the Department of Mechanical Engineering, KAIST, where he is currently a significant professor and a director of Humanoid Robot Research Center. And he has been a vice president of KAIST since 2013. He was a Visiting Research Scientist in the University of Texas Austin, from 1996 to 1997. His research interests include humanoid robots, adaptive control, intelligent control, nonlinear control, biomechanics, sensors, actuators, and application of micro- processor. Dr. Oh is a member of the IEEE, KSME, KSPE and ICASE.